HDL-8-85
ICR-Report-124-85-5

CALIBRATION OF A LIGHT SENSOR FOR BACKGROUND MEASUREMENTS IN DEEP OCEAN

T. Aoki, S. Matsuno, Y. Ohashi, A. Okada,
D. O'Connor and M. Webster

(APR. 1985. 20)

Institute for Cosmic Ray Research
University of Tokyo
Tanashi, Tokyo, Japan

CALIBRATION OF A LIGHT SENSOR FOR BACKGROUND MEASUREMENTS IN DEEP OCEAN

T.Aoki, S.Matsuno, Y.Ohashi and A.Okada
Institute for Cosmic Ray Research,
University of Tokyo, Tanashi 188, Japan

D.O'Connor
Hawaii DUMAND Center,
University of Hawaii, Manoa, USA

M.Webster
Department of Physics,
Vanderbilt University, Nashville, USA

Abstract

From the calibration of a light sensor done at Hawaii DUMAND Center, we derive detection efficiencies of photomultipliers in the light sensor and conversion factors to estimate the environmental photon flux from the counting rates of the photomultipliers at ~ one photo-electron level.

1. Introduction

The calibration of a light sensor (called JTTR) was carried out at Hawaii DUMAND Center (HDC) after the ocean experiment at the DUMAND site. The measurement of light intensity with JTTR is different from that with telemetering transient recorders, TTR-1 ~ TTR-3 (Ref.1), in the fact that it counts individual pulses from photomultiplier (PMT) higher than threshold voltages. But the calibration method we have adopted is essentially the same. We use a continuous light source, weak enough to neglect the probability of pulse overlapping, and we set the threshold voltage close to one photo-electron equivalent.

The procedure of the calibration is divided into two steps. At the first step (Fig.2), the PMT sensor was set inside a dark box , irradiated by a collimated light beam and compared with a calibrated photodiode. The purpose of this step is to check the detection efficiencies of the PMTs and the photodiode to light sources of various wave lengths. This method was already investigated in detail by the TTR members (Ref.2). Here we will mention only the present result shortly in section 3.

The second step of the calibration was done in the big water tank (Fig.3). By rotating the PMT light sensor, we obtained the effective area, expressed as [detection efficiency times sensitive area] , for various directions of incident light. Since only one color filter was used, the wave length dependence of the efficiency was not checked this time. Details of this calibration in the water tank will be presented in sections 4-7.

2. JTTR Light Sensor

The JTTR light sensor is illustrated in Fig.1, excluding a metal housing for the data acquisition. Two Hamamatsu 5" PMTs(R1391) are set inside a 17" Benthos glass sphere. The photo-cathode material is bialkali, and its sensitive surface is well approximated by a hemisphere of 5" diameter. The configuration of the dynodes is the so-called boxtype. The space gap between the inner surface of the Benthos glass sphere and the PMT photocathode surfaces is filled with

transparent silicon gel (Shinnetsu,X-32-465), the refractive index of which is 1.405. In the ocean experiment, H.V. was supplied from a DC-DC converter activated by batteries through a DC regulator. In this calibration, we used a DC power supply in place of the batteries (This statement holds also for other electronics used).

The anode pulses from each PMT are fed to individual amplifiers (two chips of LeCroy VV100B with a gain of ~ 100) in the Benthos sphere and the amplified output pulses are transmitted to each discriminator in a metal housing through coaxial cables. The threshold voltage is controlled by a micro-computer and was changed in pre-programmed time intervals in the ocean experiment. This time, we are concerned with only the lowest threshold in it (32 mV), which corresponds to $\sim$ 1/3 photo-electron (see Appendix B). Then the counting rate above this threshold is measured mainly using a conventional scaler.

3. Calibration in Air

The experimental layout is shown in Fig.2. The light source is a tungsten bulb to which a monitored current of 4.2 ampere is supplied. The light is led to the box for color filters after passing through an infra-red absorber. We can select a color filter among 12 different ones including no filter. Then the light is led to the box for neutral density filters that has 7 filters of different densities in it (density indices; "3","2","1","0.5","0.3","0.1", and "0.04", where the density index "n" means that the light intensity is attenuated by a factor of $\sim 10^{-n}$). We can select any combination of them and get a desired light intensity. The PMTs are irradiated with this outgoing light through a collimator of 1 cm^2.

We turned the light sensor properly so as to irradiate one of the PMTs just on its front. The light beam has about 4 cm diameter on the PMT. For the measurement of the absolute light intensity, a calibrated photodiode of the same sensitive area as the collimator is placed at the position of the collimator.

The counting rates of the discriminator outputs were recorded for various color filters and various combinations of the neutral density

filters, and compared with the photodiode current. Thus obtained PMT detection efficiencies are listed in Table 1.

Table 1. PMT efficiency
(Planck distribution parameter(Ref.2) : 7048.5)

Filter	Average Wave Length	Efficiency PMT-1	Efficiency PMT-2	Ratio to J.Learned Curve PMT-1	Ratio to J.Learned Curve PMT-2
25-400	403 nm	(38.9 %)	(47.4 %)	(1.64)	(2.00)
03FIB002	434 nm	25.6 %	31.6 %	1.18	1.46
25-450	451 nm	26.6 %	33.2 %	1.32	1.65
03FIB004	475 nm	23.8 %	29.7 %	1.36	1.69
03FIB003	492 nm	18.3 %	23.5 %	1.19	1.52
25-500	501 nm	17.4 %	24.6 %	1.24	1.75
03FIV027	522 nm	10.4 %	13.2 %	0.90	1.14
25-550	551 nm	6.5 %	8.8 %	0.92	1.24
25-600	603 nm	(1.1 %)	(2.1 %)	(0.65)	(1.29)

The color filters listed up are restricted to those which proved to be reasonable concerning photodiode responses. From this point of view, the most reliable four data are those of 03FIB002, 25-450, 03FIB004 and 03FIB003 (see Ref.2 about the degree of reliability defined as 'RATIO'). The PMT efficiencies in the table are based on Webster's calculation (Ref.2), slightly modified for the neutral densities remarked in Appendix A.

A typical quantum efficiency offered by Hamamatsu Photonics is shown in Fig.8 (BIALKALI:A). Our detection efficiency looks a little high compared to this and also to the Learned curve (Ref.2). Moreover, since we did not take into account the light absorption in the Benthos glass ($\sim$ 10 %) and in the gel, the net efficiency of PMT could be higher.

4. Calibration in Water Tank

The arrangement of calibration in a water tank is shown in Fig.3. A slide projector was used as the light source because of its high intensity. As color filter, 03FIB003 (460 nm wide band) was uniquely selected, also because this allows the brightest light, necessary for an accurate measurement of the photodiode current. The character of the diffusing ball had been checked by HDC experts. The light intensity yielded is uniform against the horizontal rotation and depends slightly on the vertical rotation. But practically this gives no significant influence on the present data, being confirmed by the data itself.

In the ocean experiment, the light sensor was supported by a aluminium frame structure. To reproduce the sensitive area, the same pieces of frame are used around the sensor as far as they have any possibility to interrupt incoming lights. But to make the whole sensor (with the frame) rotatable, we had to add an extra frame newly, which can also interrupt light in some cases and lead to a lower estimate of the sensitive area. We have to subtract this effect in the data analysis. The newly added frame does not move with the Θ rotation, but moves together with the Φ rotation. The definitions of Θ and Φ are given in the following.

5. Result of Water Tank Calibration

Now we define Θ as the vertical rotation angle and Φ as the horizontal rotation angle, where $\Theta=0^\circ$ and $\Phi=0^\circ$ corresponds to such a sensor position that its front faces just the diffusing ball. When $\Theta=90^\circ$, the sensor is looking upwards.

It took six days to survey measurements of counting rates at every $\sim 10^\circ$ for Θ and every $\sim 5^\circ$ for Φ. Background measurement ('light-off') was also done at some (Θ, Φ) points. This background counting rate decreased gradually with time for the first two or three days. In Fig.4 the background rates are shown on (Θ,Φ) plane, divided into the first three days and the latter three days. The diameters of circles in the figure are proportional to deviations from 3.0 KHz for

PMT-1 and 2.5 KHz for PMT-2, and the full circles indicate negative deviations. The background consists of PMT dark noise and Cerenkov signals from muons passing through the water tank (no light leakage from outside the tank). The arrows in Fig.4 indicate those areas on (θ,Φ) where the distance between PMTs and the wall of the tank is closest and so the muon contribution to the counting rate is minimized. The subtraction of this minimum counting rate from the maximum one gives a rough estimate of the muon contribution; 0.6 KHz for PMT-1 and 1.0 KHz for PMT-2. Each data, when the light was on ('light-on'), was corrected by subtracting the corresponding light-off data closest on (θ,Φ) plane.

As to the light-on data, we repeated the measurement on the last day picking up some points on (θ,Φ) from previously measured data in order to check the stability of the light source. Shown in Fig.5 is the time variation of the counting rate relative to the re-measured one. During data taking, we recognized that the AC voltage supplied to the slide projector (light source) was not always constant. So we used a slidetrans from that time on and tried to keep the voltage constant manually. But from the figure, there seems to be still some time dependence. Except for the first day, the counting rate decreases gradually. We can not say exactly whether this tendency is due to the decrease of the light source intensity or due to some other reason, for instance, attachment of some contamination in water on the glass sphere. We should have monitored the light intensity continuously by a photo-diode. However, we have monitored as far as DC power supplies are concerned and we are sure that HV to the PMTs, amplifier gains and discriminator threshold voltages were kept constant. So we corrected all 'light-on' data by normalizing them to the re-measured data.

Thus obtained data about PMT-1 are indicated by circles in Fig.6. We have of course PMT-2 data, although not shown here explicitly. For all these data, the indices of the neutral density filters are '3' plus '2', which means accurately an attenuation of $10^{-4.886}$ times the light intensity for such a region of wave length as characterized by the color filter 03FIB003 (Ref.2). On the other hand, the photo-diode current on the last day was 0.275 nanoampere without the neutral density filters. This is equivalent to a flux of $2.46 \cdot 10^9$ photons $/cm^2/sec$ on the photodiode.

6. Calculation of PMT Sensitive Area

To determine the photon absolute intensity at DUMAND site, we need to know the quantity of [the total geometrical acceptance times PMT detection efficiency] . The whole measured data is not abundant yet to get the quantity directly because of the too coarse interval of sampling angles compared to the complex frame structure. So, in order to estimate counting rates at the intermediate angles, we calculated numerically the sensitive solid angle of PMT as a function of the rotation angles for the calibration layout.

In the calculation we assumed :

1) point-like and isotropic light source (the diffusing ball).
2) refraction of light incident on the glass sphere (n = 1.475, assumed) and into the gel (n = 1.405), and no reflection there.
3) total reflection at the gel surface not bordered by the Benthos glass or PMTs, when the angle of incidence on the surface from inside the gel is larger than the critical angle (45°).
4) no reflection on any piece of the frame.
5) no transparency of photo-cathodes.
6) angular dependence of PMT relative efficiency,
   $(1 + 0.15 \cdot \sin\theta\cos\varphi)$ for PMT-1 and
   $(1 + 0.10 \cdot \sin\theta\cos\varphi)$ for PMT-2.
   This correction of efficiencies is included in the effective solid angle. Here, θ and φ are conventional definitions (different from Θ and Φ), where $\theta=0°$ corresponds to the front of PMT, $\theta=90°$ does to the equator and φ stands for the longitude.

The calculated solid angles are multiplied by a constant, which must correspond to [PMT efficiency times photon flux /sr /sec] ;
$1.075 \cdot 10^7$ for PMT-1,
$1.775 \cdot 10^7$ for PMT-2,
and are compared with data in Fig.6 (solid lines). The quality of the fit is good. For PMT-2, not shown here, it is almost as good as for PMT-1. The complex feature commonly seen around $\Phi=90°$ in Fig.6 is

due to the newly added frame.

Now we can derive the PMT detection efficiency. The photon flux on the photodiode is given in section 5. Taking into account the neutral density filters used for PMT and the distance of 56.5 cm between the diffusing ball and the photodiode, we get;

photon flux on PMT = $1.02 \cdot 10^8$ /sr/sec.

Therefore from the above constants;

PMT efficiency = 10.5 % for PMT-1,

= 17.4 % for PMT-2.

Since these overall efficiencies include the collection efficiency as well as the quantum efficiency, this result is not inconsistent with that in Table 1 where we used the collimated light illuminating right the PMT front. The averaged efficiency all over the photocathode may be worse. On the other hand, we might over-estimate the sensitive solid angle. It is doubtful whether all the assumptions made above are valid. For example, the reflection of light on the glass sphere increases actually when the light path is inclined. For the final aim mentioned in the next section, however, we do not need to know both the efficiency and the solid angle independently. We need only their product.

7. Uniform photon flux vs. Counting Rate

Since the calculated solid angles (i.e. sensitive areas in case of a parallel light beam) is in good proportion to the measured data, the total geometrical acceptance can be derived by simply performing the numerical integration over every direction. Here the newly added frame has to be taken away in the calculation, because we are now concerned with the ocean measurement.

The θ dependence of the sensitive area /sr averaged over φ is shown in Fig.7 and the total geometrical acceptance is 520 cm^2sr. This total geometrical acceptance is almost independent of the light source distance from the sensor, within 2 % except at very short distances (< 30 cm). So the uniform photon intensity is given by ;

I (photons /$cm^2 \cdot$ sr $\cdot$ sec) = [counting rate] /54.6 for PMT-1,

I (photons /$cm^2 \cdot$ sr $\cdot$ sec) = [counting rate] /90.5 for PMT-2,

or,

I (photons /cm^2 · sec) = [counting rate] /17.4 for PMT-1,

I (photons /cm^2 · sec) = [counting rate] /28.8 for PMT-2.

At the time of the ocean experiment, we failed to record the rotational position of the PMTs relative to the square frame in its topview. Later we removed the sensor out of the frame and replaced it again for the calibration. So, the geometrical acceptance might have changed. But from the calculation, the error caused is less than ± 1 %. The most significant error comes from the geomagnetic effect (~ 10 %, see Appendix B). A similar or smaller amount of error could have arisen from the conversion of photon flux from the photodiode to the PMTs. Besides, what we feel a little anxious about are the actual values of the neutral density filters mounted in the filter box, because higher density filters among them are hardly examined by our available method.

Acknowledgement

We would like to thank Mr.M.McMurdo and Mr.D.Harris for their helps on the mechanics in the water tank and the data transmission to the host computer, respectively. We are also grateful to Prof.J.Learned, Prof.T.Kitamura, Dr.C.Wilson and Prof.C.Grupen for their advisable discussions. This work was done by utilizing facilities at HDC and Hawaii Institute for Geophysics, and a part of the analysis was carried out with the computer of Institute for Nuclear Study in University of Tokyo.

Reference

1) H.Bradner et al.; Nature (in press)

2) S.Matsuno, D.O'Connor, J.Clem, M.Bartlett and M.Webster ; DUMAND Internal Report, DIR 13-83

3) The JTTR result is to be submitted elsewhere.

Appendix A : Comment on Neutral Density Filters

We can measure densities of some neutral density filters by comparing PMT counting rates with and without each filter in question for the apparatus shown in Fig.2. Of course we have to assume a linearity between the counting rate and the light intensity onto PMT. So it is hard to apply this method to higher density filters (density indices "2", "3").

The results for the indices "1", "0.5" and "0.3" are shown in Fig.A1 together with the expected values which were calculated from the filter characteristics supplied by the company (Ref.2). The large dispersion of data seen in Fig.A1(b) is not due to any measurement error nor any instrumental fluctuation, e.g. that of PMT gain. We have repeated the measurement two or three times at each data point on different occasions for both PMTs, and the error is typically .003. That large dispersion is also not due to the saturation of PMT at high light intensity. The deviation of data from the expected value is plotted in Fig.A2 against the mean of the two PMT counting rates used to derive the data. The data points do not simply depend on the counting rate of PMT at least < 100 KHz.

They seem to depend rather on the combination of the neutral density filters being used. For the examination of a certain filter, other filters are commonly used to get the proper light intensity. In Fig.A1(b), the full circles indicate that the filter of index "1" is used as one of the common filters and for the open circles not. Similarly, in Fig.A1(c) the full circles indicate the common use of the index "0.5". These two figures seem to suggest some correlation between the filters of "0.5" and "1".

In Fig.A3 are shown examples of linear relations between the counting rate and the light intensity. The latter is expressed relatively as the fraction of light passing through the density filters used. Here the squares correspond to uncorrected densities and the full circles to corrected ones assuming the above correlation;

"1" -----> (expected value) with "0.5"
-----> (expected value - 0.05) without "0.5"
"0.5" ---> (expected value - 0.012) with "1"
---> (expected value - 0.067) without "1"

Figure Captions

Fig.1 : JTTR LIght sensor. Above the level of the silicon gel surface nearly equal to the borderline of photo-cathode, the glass sphere is covered with black adhesive tape.

Fig.2 : Arrangement for the calibration in air. All equipments except for the light sensor in the box are available at HDC.

Fig.3 : Layout for the calibration in water. The filter box is the the same as that in Fig.2. The water tank is cylindrical with diameter of ~ 3 m and height of ~ 2 m.

Fig.4 : Background counting rates on (θ,Φ) plane (see section 5 for θ and Φ). The diameters of circles are proportional to deviations from 3.0 KHz for PMT-1 and 2.5 KHz for PMT-2, and the full circles indicate negative deviations.

Fig.4(a) --- PMT-1, dates of 9/27 - 9/29/84

Fig.4(b) --- PMT-1, dates of 9/30 - 10/2/84

Fig.4(c) --- PMT-2, dates of 9/27 - 9/29/84

Fig.4(d) --- PMT-2, dates of 9/30 - 10/2/84

Fig.5 : Relative light intensities (more precisely, relative counting rates under fixed conditions of the filters and the rotation angles of the light sensor) varying with time.

Fig.6 : Counting rates of PMT-1 on various rotational angles of θ and Φ. In a graph, θ is fixed. Solid lines show numerical calculations under the assumptions in text.

Fig.7 : Calculated sensitive area of one of the PMTs in the sensor shown in Fig.1 versus θ, averaged over φ. A dip seen in the curve is due to the triangular plates on the front plane of the frame.

Fig.8 : Typical quantum efficiencies offered by Hamamatsu Photonics. The curve denoted by BIALKALI-A is our case.

Fig.A1 : Measured optical densities for three neutral density filters against various wave lengths. Dashed lines are expected densities. Names of color filters are listed up at the bottom column along with arrows indicating their own mean wave lengths.
Fig.A1(a) --- for neutral density filter of index "0.3"
Fig.A1(b) --- for neutral density filter of index "0.5"
Fig.A1(c) --- for neutral density filter of index "1"
Here, open circles denote data of "0.5" (or "1") measured under the condition that the other filter "1" (or "0.5") is off.

Fig.A2 : Deviations of measured optical densities of "0.5" from expected values versus counting rates of the PMTs. This figure indicates that the splitting measured densities can not be simply explained by the saturation of PMT.

Fig.A3 : Examples of counting rate against attenuation of light obtained using neutral density filters.

Fig.B1 : Ratios of the counting rates at discriminator threshold of 20 to that of 4 on (θ,φ) plane for PMT-1. The size of square is proportional to the ratio.

Fig.B2 : Integral pulse height distributions of the PMTs in three different cases, i.e. the calibration in air, the calibration in water and the measurement in deep ocean.

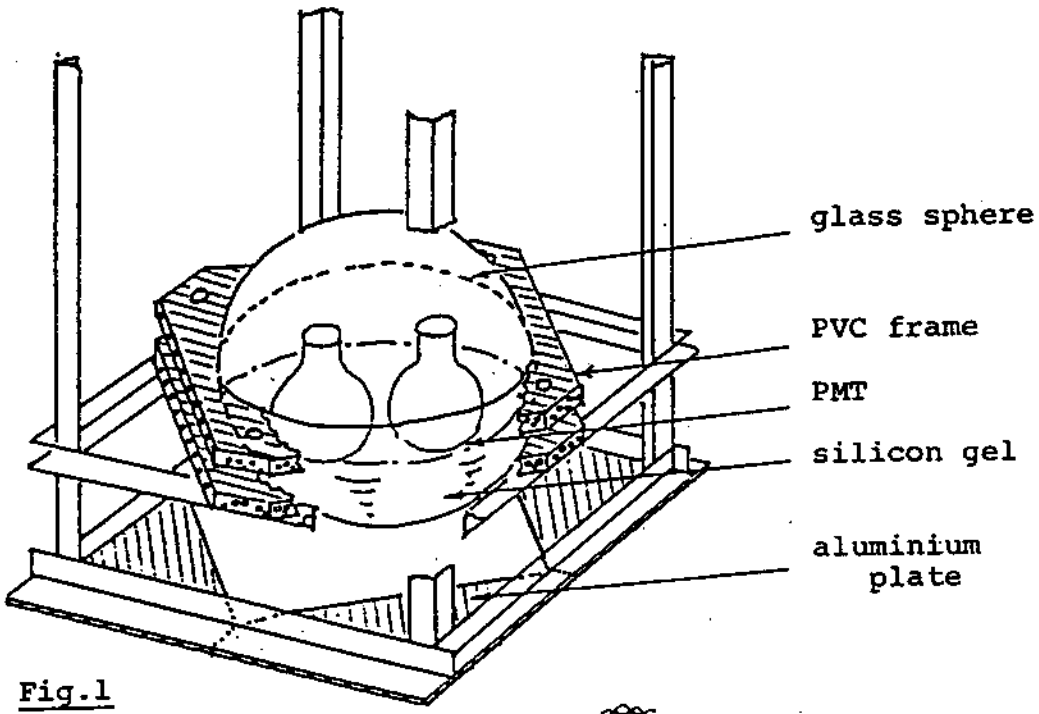
glass sphere
PVC frame
PMT
silicon gel
aluminium plate

Fig.1

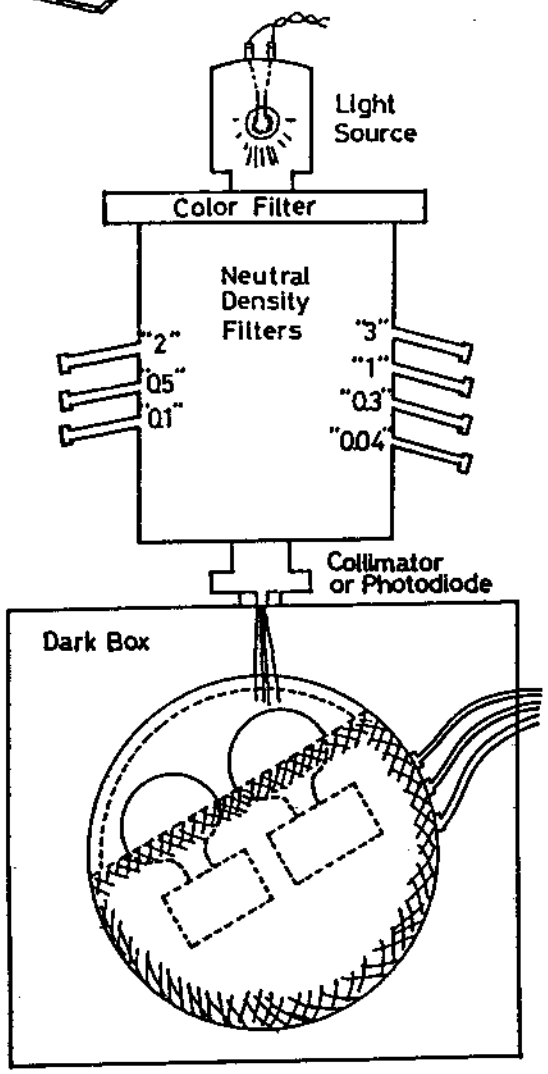
Light Source
Color Filter
Neutral Density Filters
"2"
"0.5"
"0.1"
"3"
"1"
"0.3"
"0.04"
Collimator or Photodiode
Dark Box

Fig.2

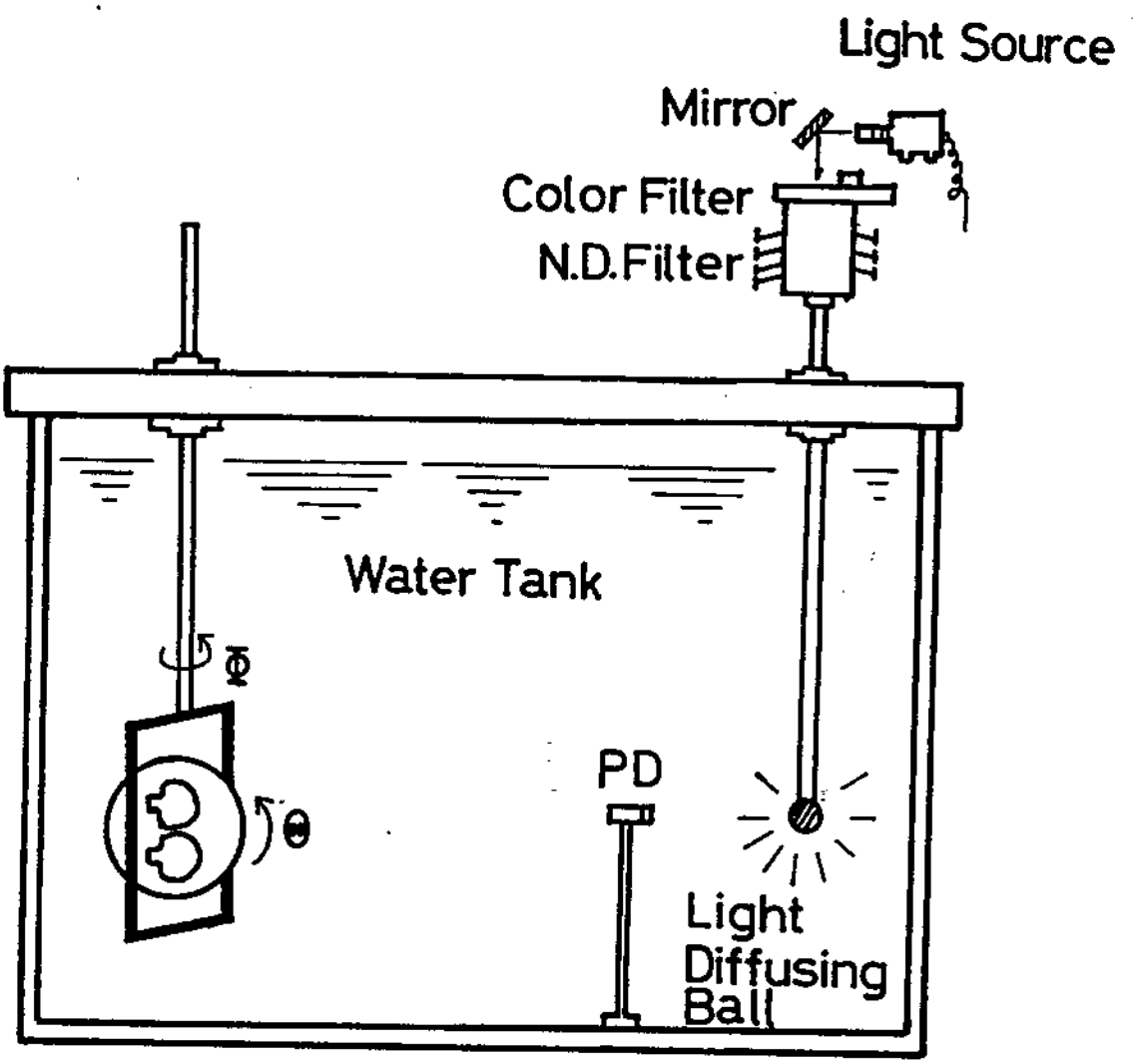
Light Source
Mirror
Color Filter
N.D.Filter
Water Tank
Φ
θ
PD
Light
Diffusing
Ball

Fig.3

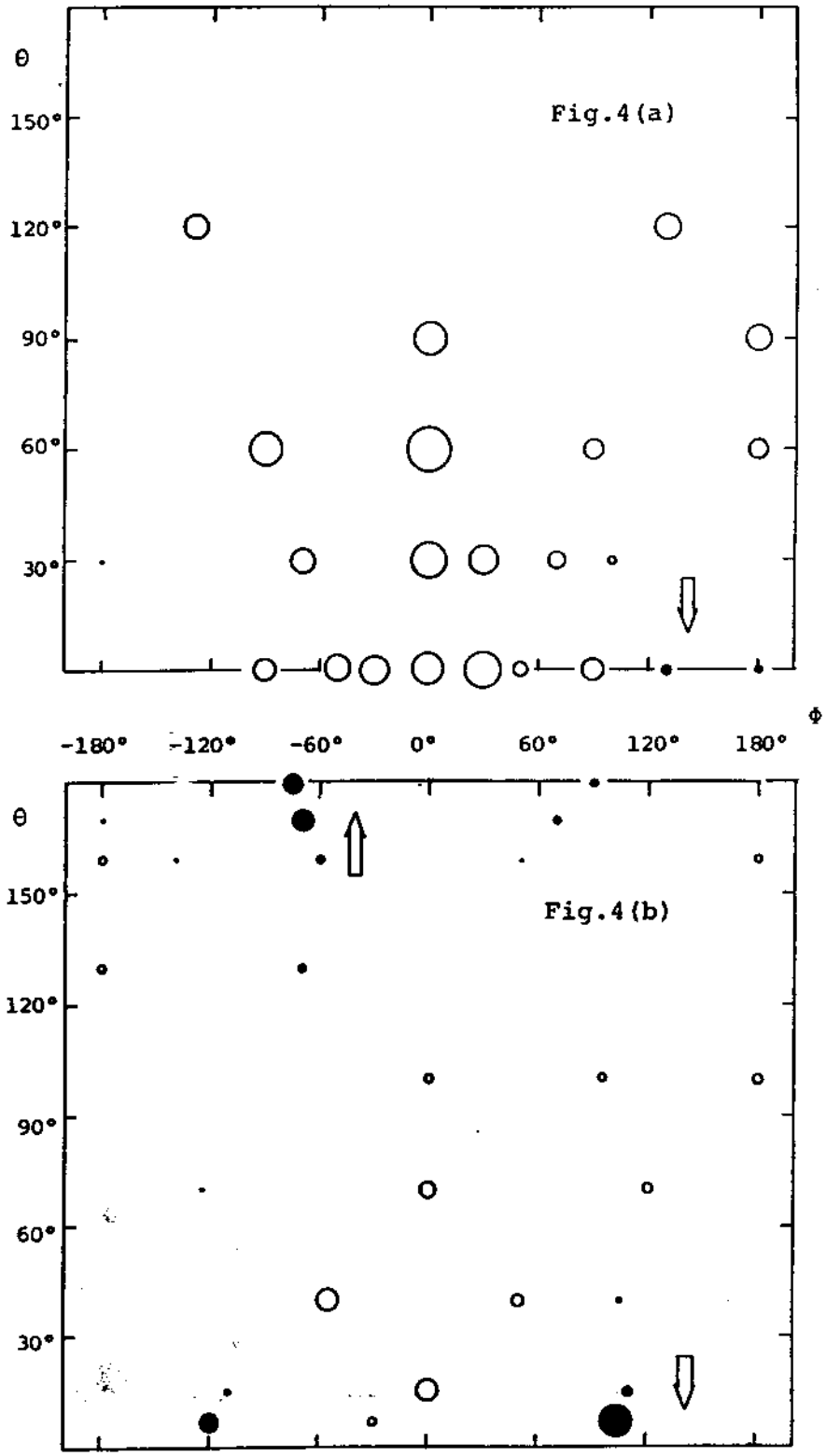
θ
150°
120°
90°
60°
30°
Fig.4(a)
-180°
-120°
-60°
0°
60°
120°
180°
Φ
θ
150°
120°
90°
60°
30°
Fig.4(b)

Fig.4

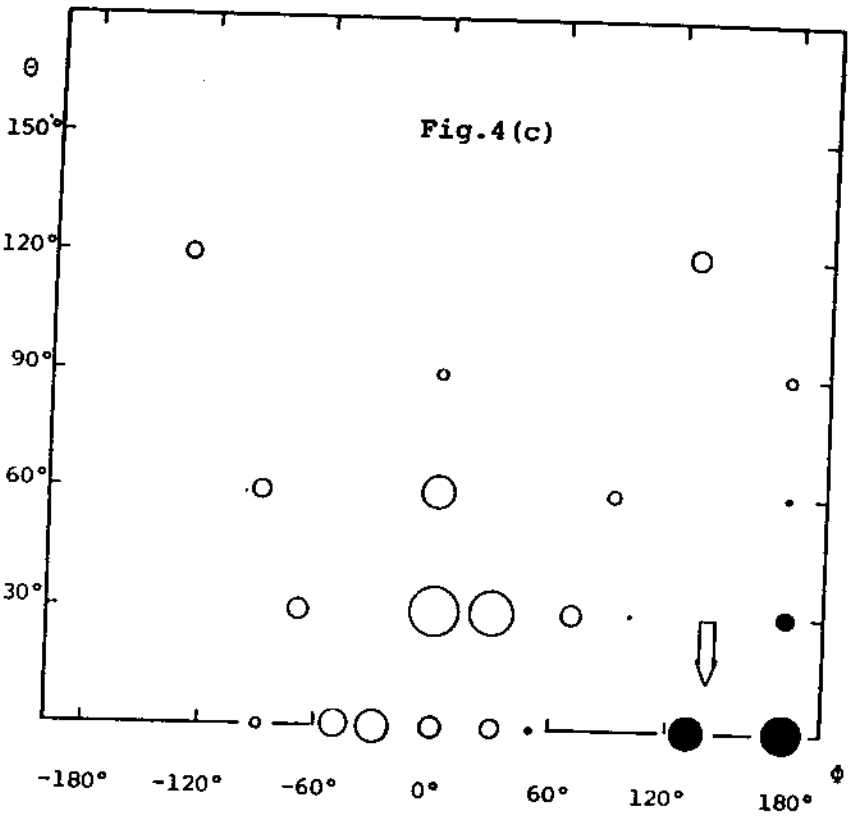

Fig.4(c)

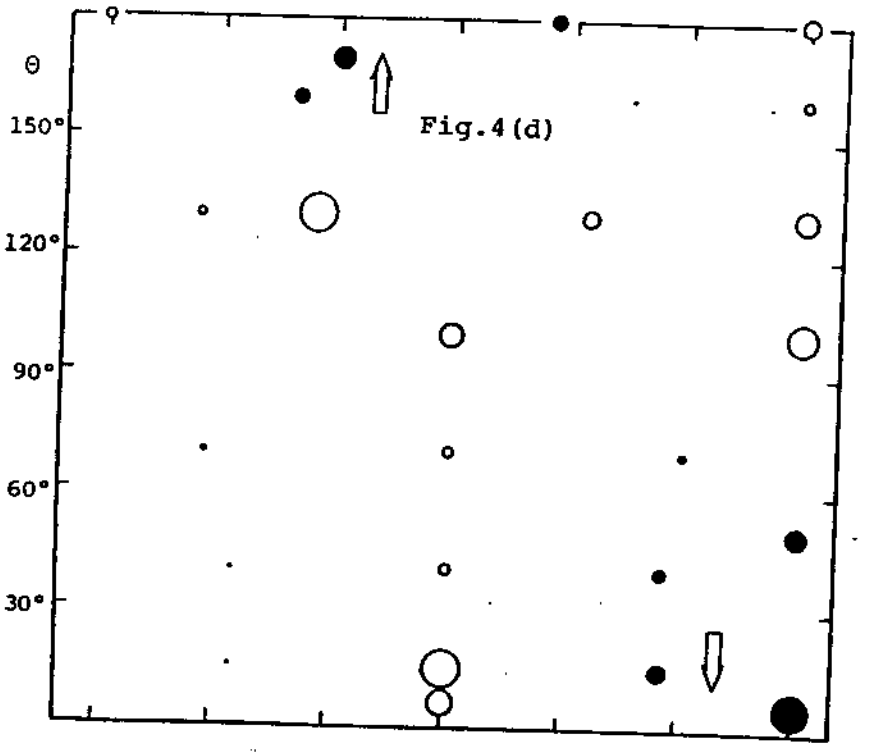

Fig.4(d)

Fig.5

Time Variation of Light Intensity
(from the Slide Projector)

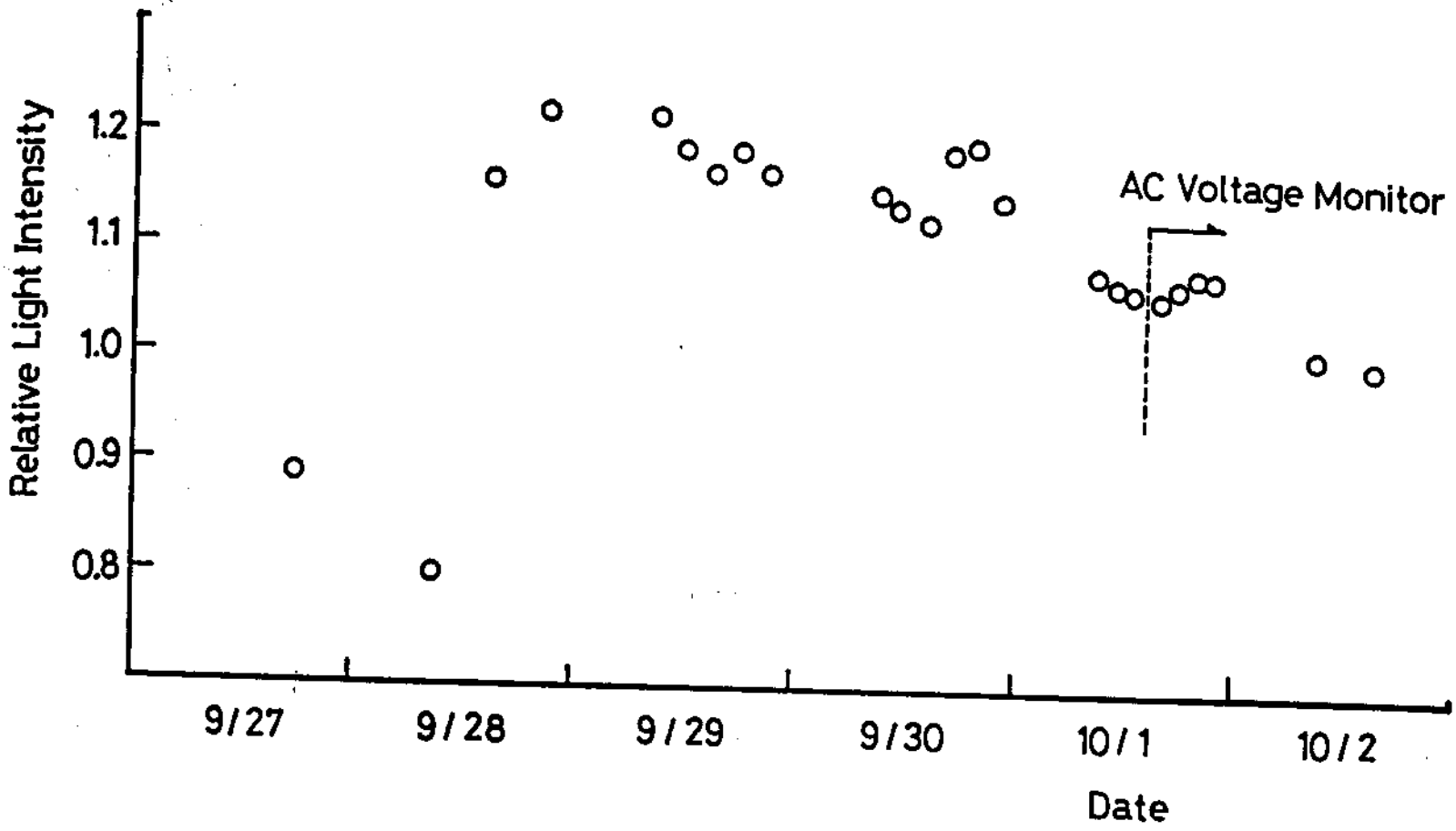

Fig.6

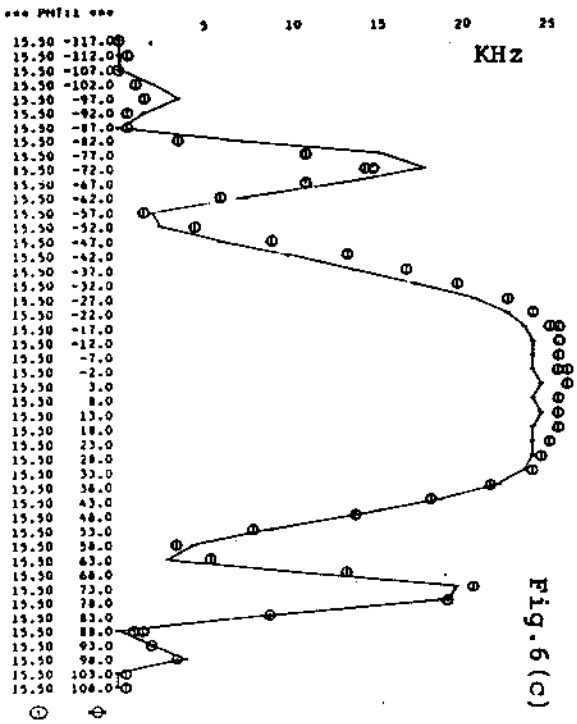

Fig.6(c)

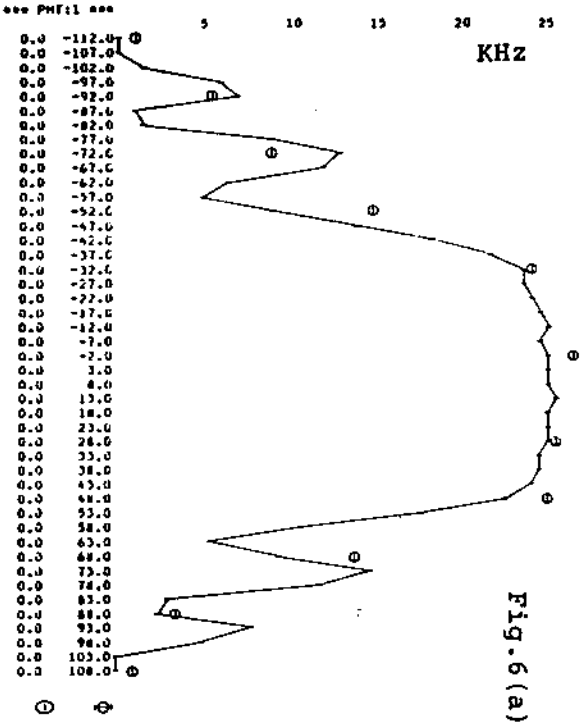

Fig.6(a)

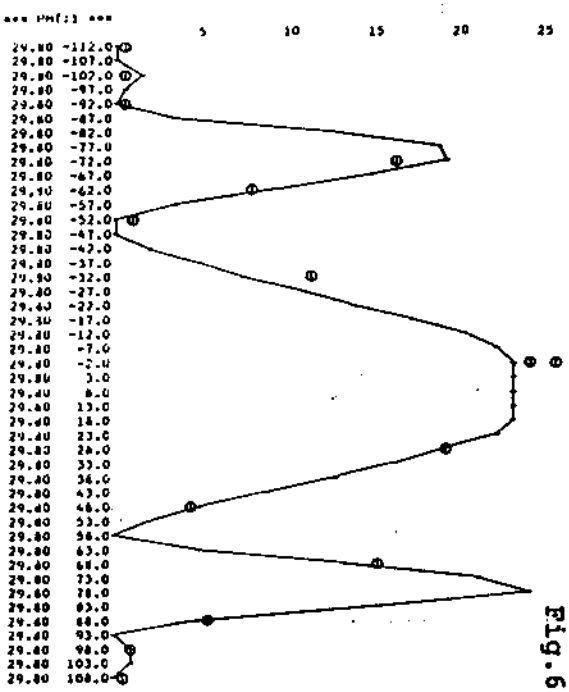

Fig.6(d)

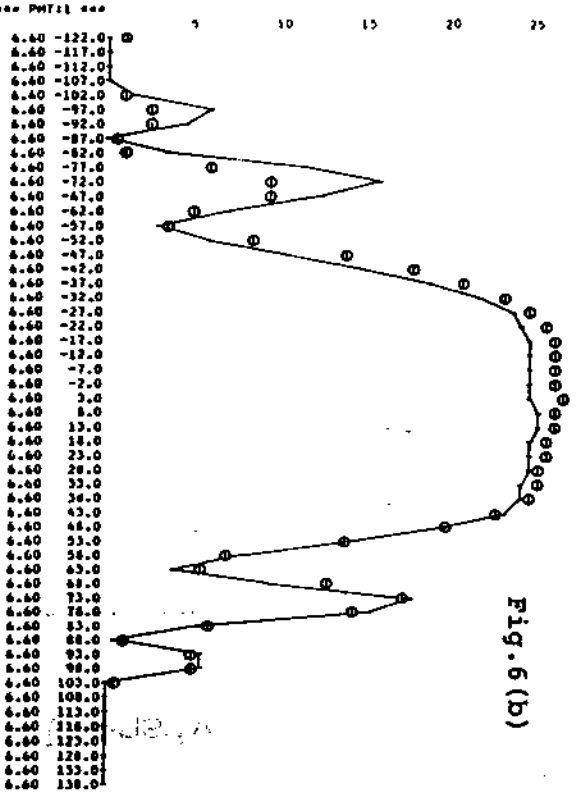

Fig.6(b)

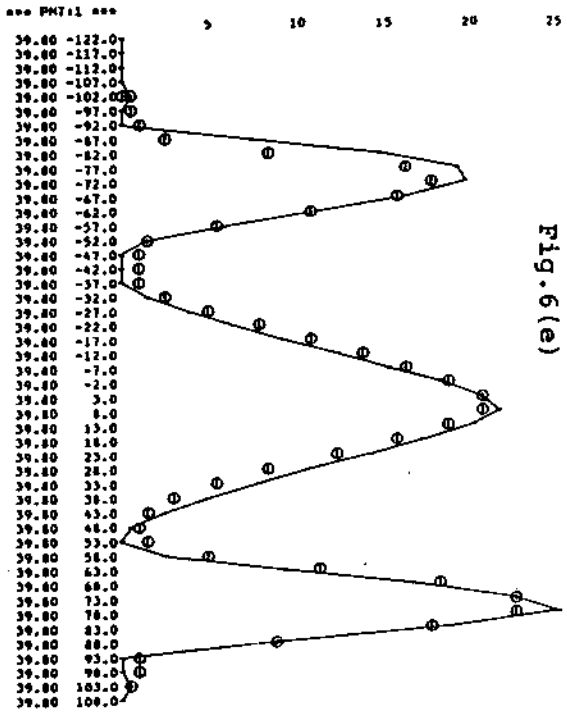

Fig.6(e)

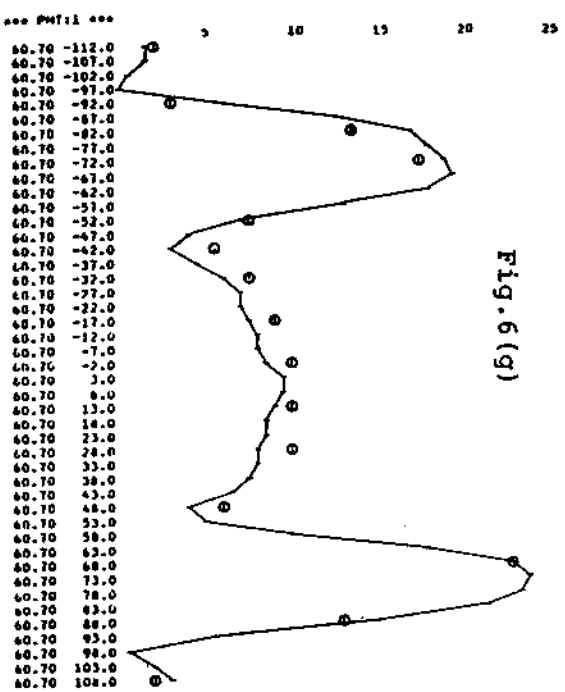

Fig.6(g)

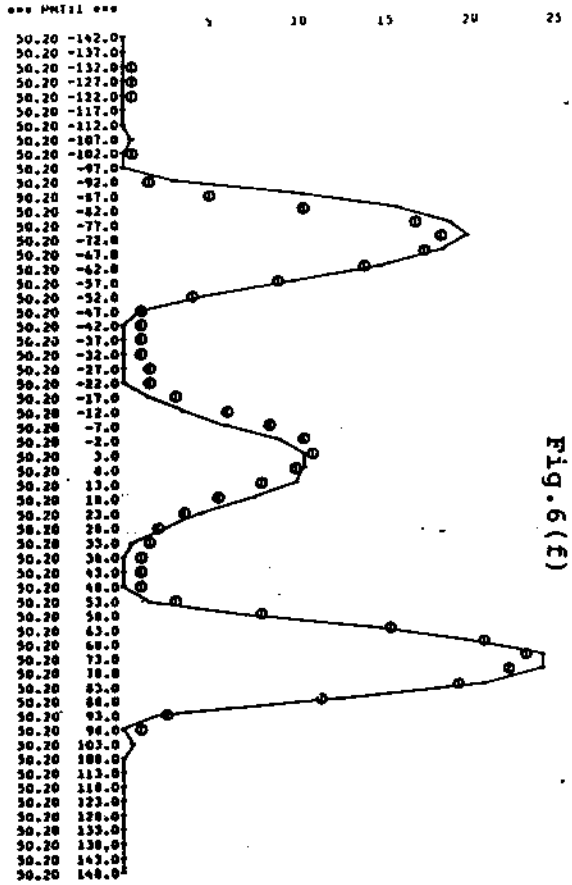

Fig.6(f)

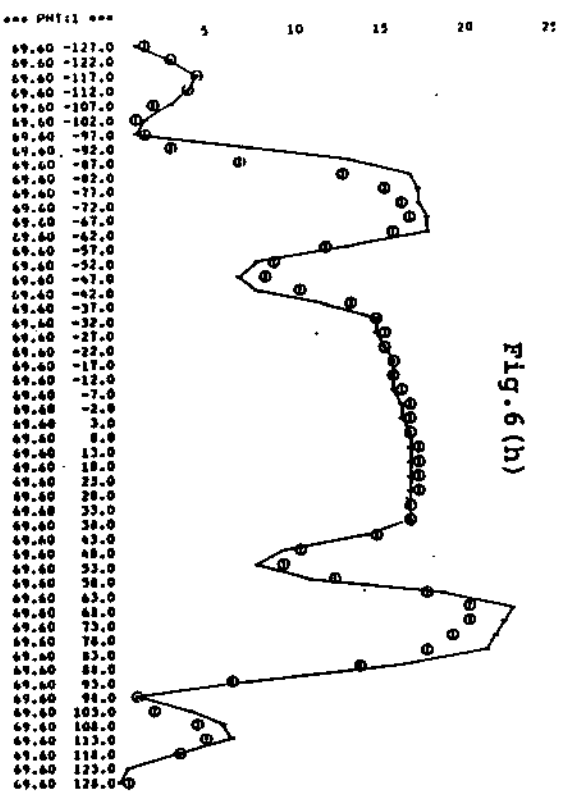

Fig.6(h)

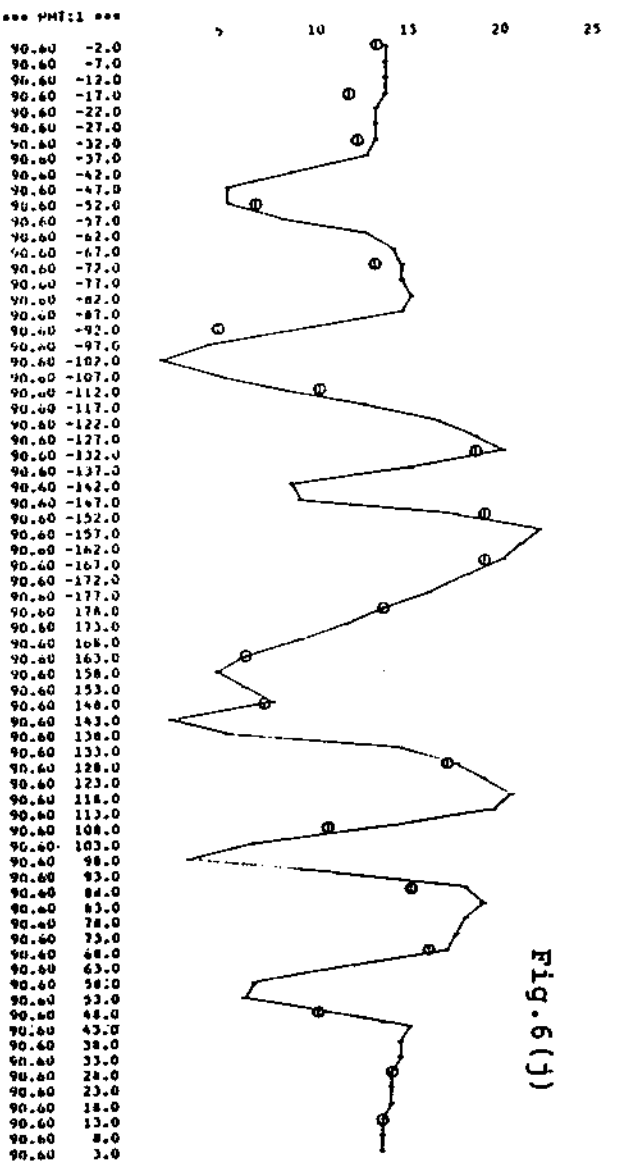
*** PMT:1 ***
90.60 -2.0
90.60 -7.0
90.60 -12.0
90.60 -17.0
90.60 -22.0
90.60 -27.0
90.60 -32.0
90.60 -37.0
90.60 -42.0
90.60 -47.0
90.60 -52.0
90.60 -57.0
90.60 -62.0
90.60 -67.0
90.60 -72.0
90.60 -77.0
90.60 -82.0
90.60 -87.0
90.60 -92.0
90.60 -97.0
90.60 -102.0
90.60 -107.0
90.60 -112.0
90.60 -117.0
90.60 -122.0
90.60 -127.0
90.60 -132.0
90.60 -137.0
90.60 -142.0
90.60 -147.0
90.60 -152.0
90.60 -157.0
90.60 -162.0
90.60 -167.0
90.60 -172.0
90.60 -177.0
90.60 178.0
90.60 173.0
90.60 168.0
90.60 163.0
90.60 158.0
90.60 153.0
90.60 148.0
90.60 143.0
90.60 138.0
90.60 133.0
90.60 128.0
90.60 123.0
90.60 118.0
90.60 113.0
90.60 108.0
90.60 103.0
90.60 98.0
90.60 93.0
90.60 88.0
90.60 83.0
90.60 78.0
90.60 73.0
90.60 68.0
90.60 63.0
90.60 58.0
90.60 53.0
90.60 48.0
90.60 43.0
90.60 38.0
90.60 33.0
90.60 28.0
90.60 23.0
90.60 18.0
90.60 13.0
90.60 8.0
90.60 3.0
5
10
15
20
25

Fig.6(j)

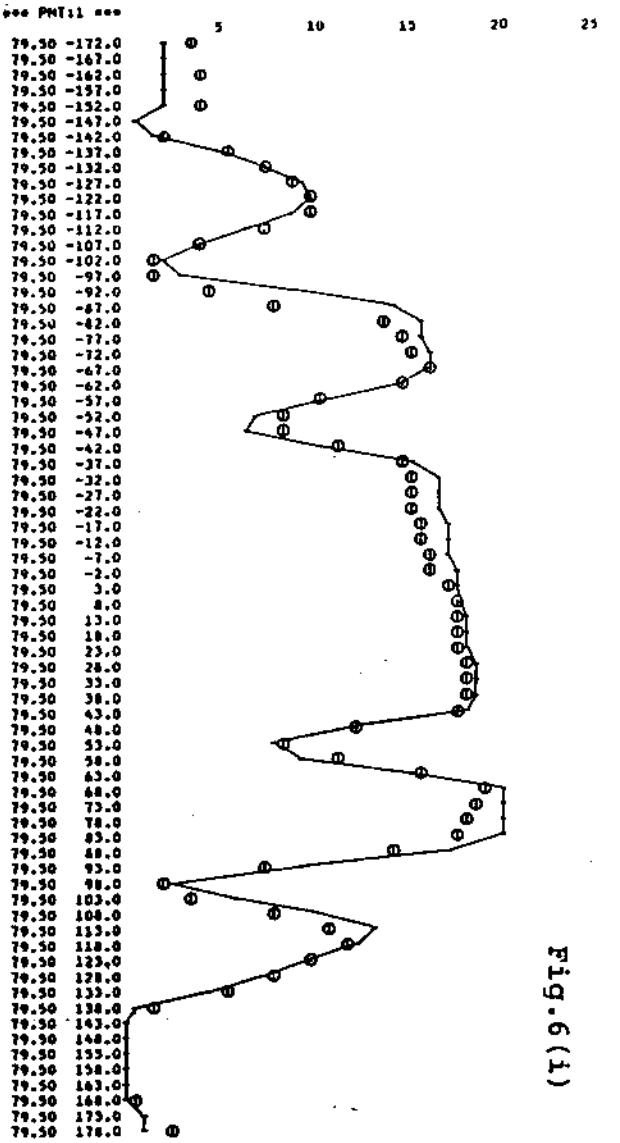
*** PMT:1 ***
79.50 -172.0
79.50 -167.0
79.50 -162.0
79.50 -157.0
79.50 -152.0
79.50 -147.0
79.50 -142.0
79.50 -137.0
79.50 -132.0
79.50 -127.0
79.50 -122.0
79.50 -117.0
79.50 -112.0
79.50 -107.0
79.50 -102.0
79.50 -97.0
79.50 -92.0
79.50 -87.0
79.50 -82.0
79.50 -77.0
79.50 -72.0
79.50 -67.0
79.50 -62.0
79.50 -57.0
79.50 -52.0
79.50 -47.0
79.50 -42.0
79.50 -37.0
79.50 -32.0
79.50 -27.0
79.50 -22.0
79.50 -17.0
79.50 -12.0
79.50 -7.0
79.50 -2.0
79.50 3.0
79.50 8.0
79.50 13.0
79.50 18.0
79.50 23.0
79.50 28.0
79.50 33.0
79.50 38.0
79.50 43.0
79.50 48.0
79.50 53.0
79.50 58.0
79.50 63.0
79.50 68.0
79.50 73.0
79.50 78.0
79.50 83.0
79.50 88.0
79.50 93.0
79.50 98.0
79.50 103.0
79.50 108.0
79.50 113.0
79.50 118.0
79.50 123.0
79.50 128.0
79.50 133.0
79.50 138.0
79.50 143.0
79.50 148.0
79.50 153.0
79.50 158.0
79.50 163.0
79.50 168.0
79.50 173.0
79.50 178.0
5
10
15
20
25

Fig.6(i)

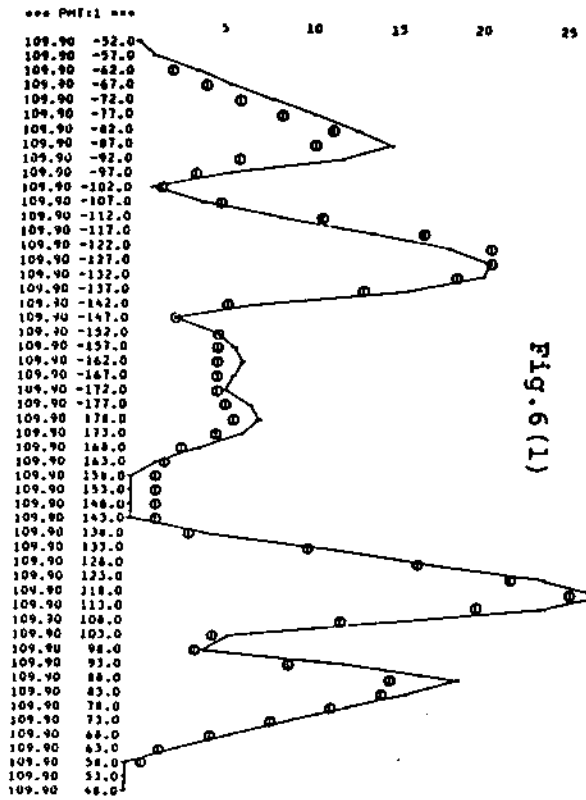

Fig.6(l)

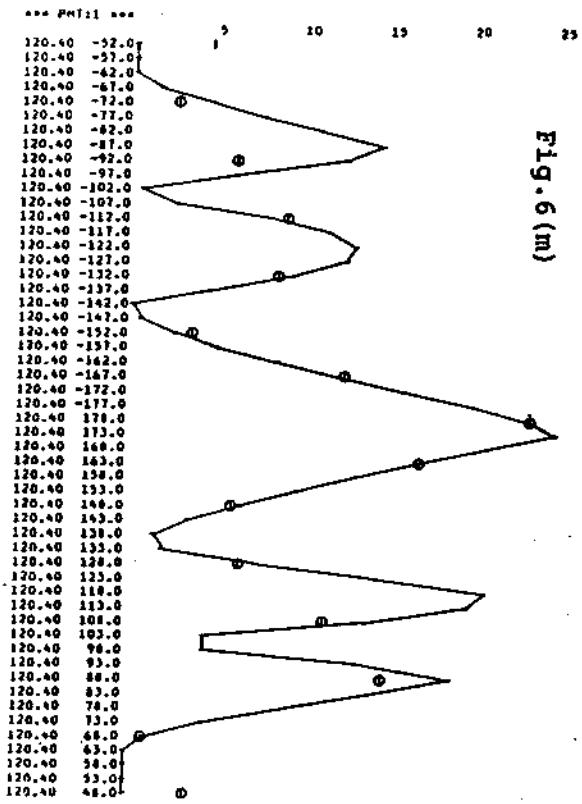

Fig.6(m)

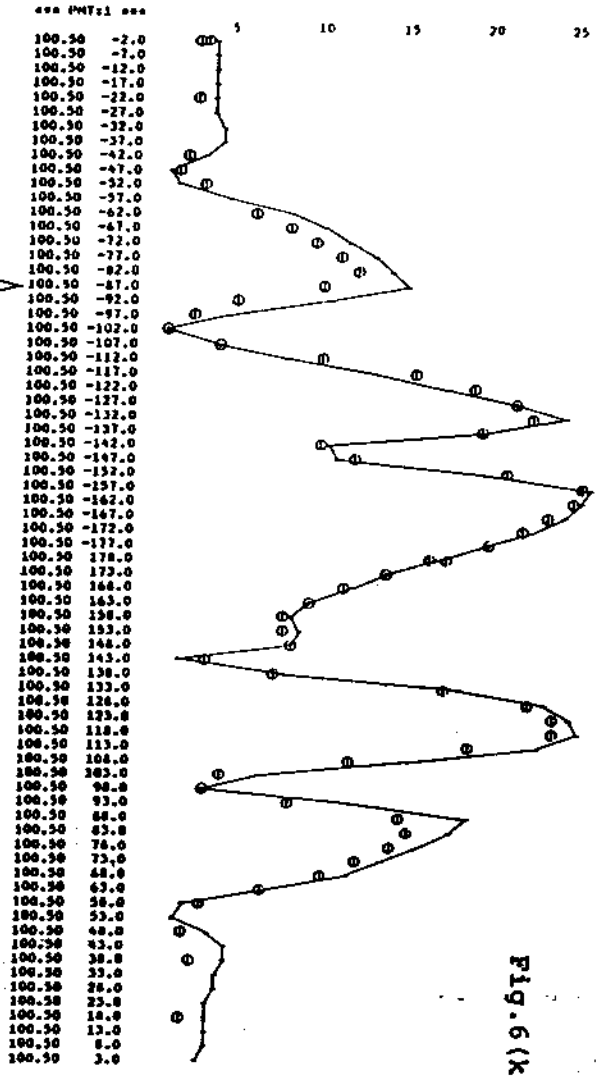

Fig.6(k)

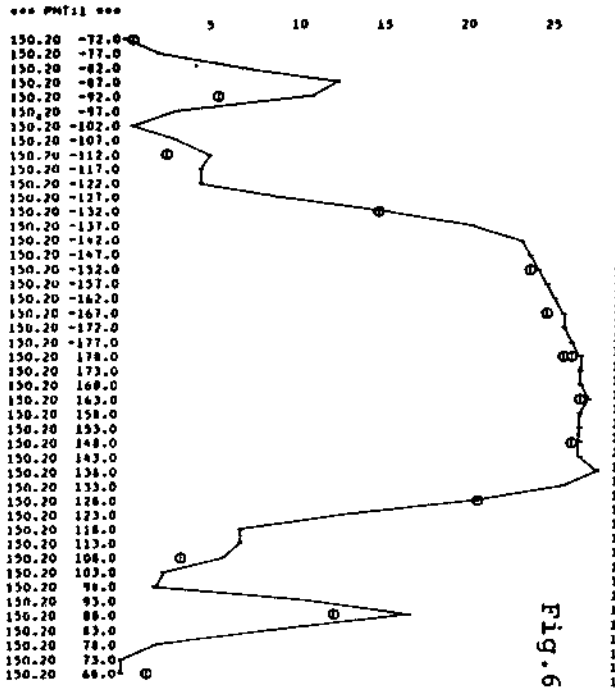

Fig.6(p)

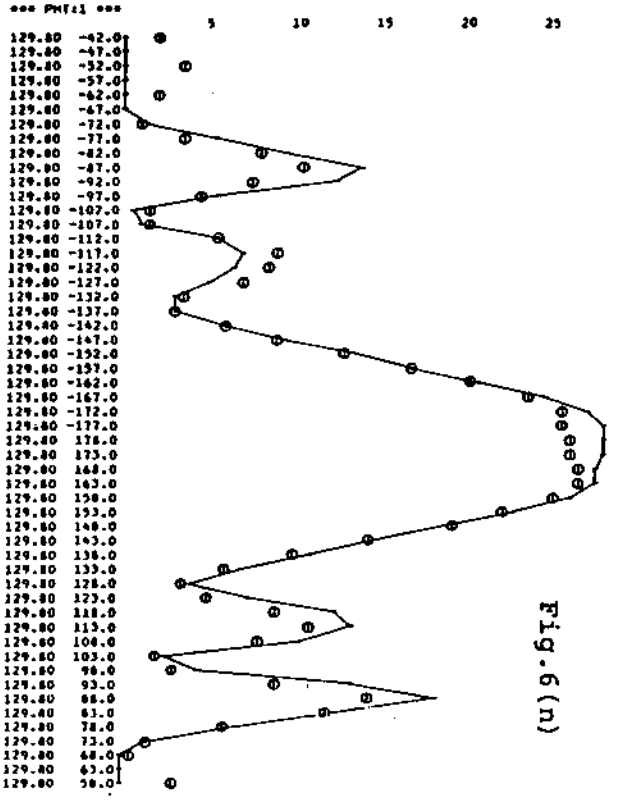

Fig.6(n)

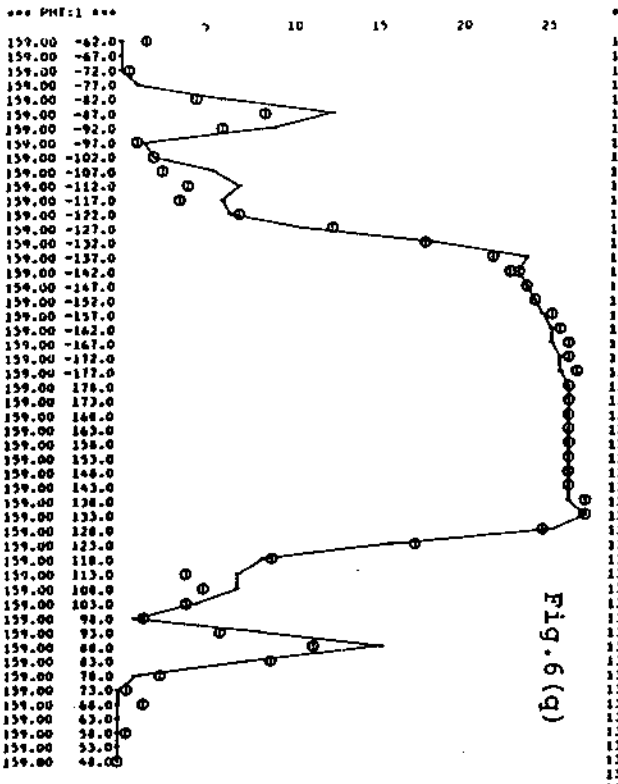

Fig.6(q)

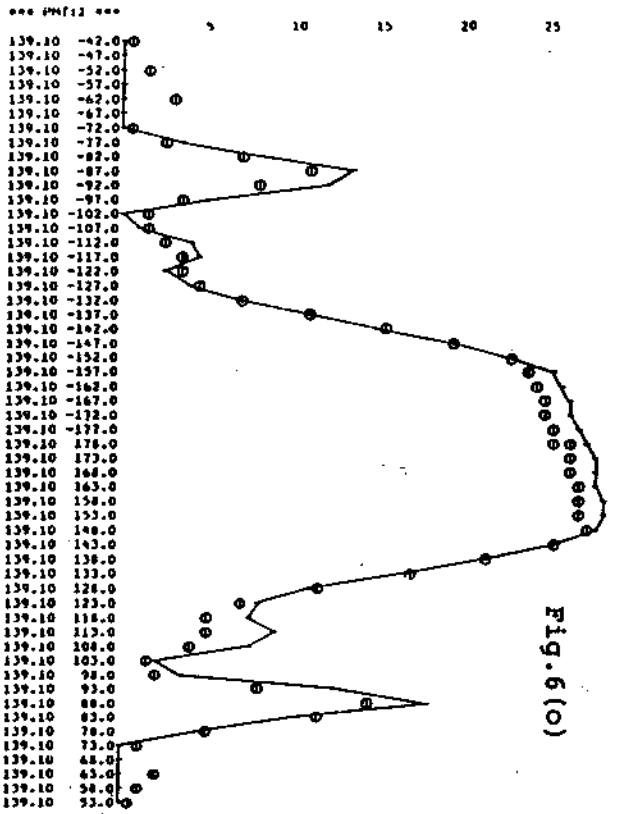

Fig.6(o)

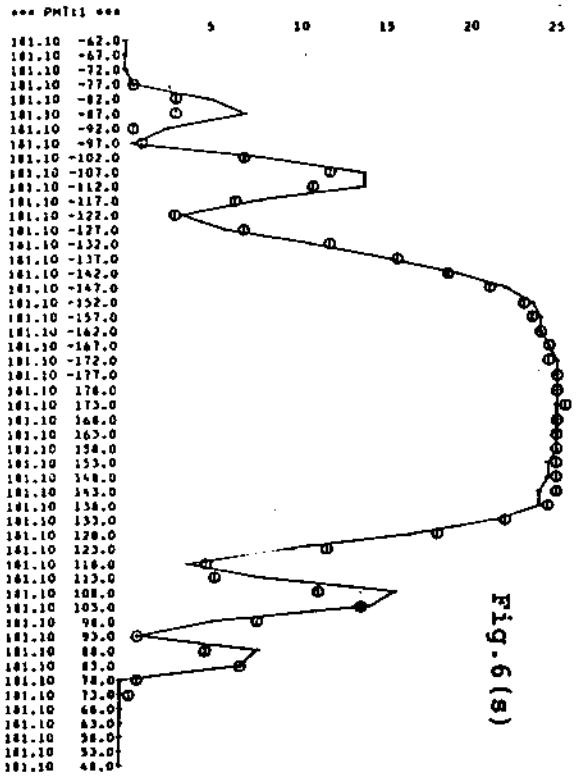
*** PHI:1 ***
5
10
15
20
25
181.10 -62.0
181.10 -67.0
181.10 -72.0
181.10 -77.0
181.10 -82.0
181.10 -87.0
181.10 -92.0
181.10 -97.0
181.10 -102.0
181.10 -107.0
181.10 -112.0
181.10 -117.0
181.10 -122.0
181.10 -127.0
181.10 -132.0
181.10 -137.0
181.10 -142.0
181.10 -147.0
181.10 -152.0
181.10 -157.0
181.10 -162.0
181.10 -167.0
181.10 -172.0
181.10 -177.0
181.10 176.0
181.10 173.0
181.10 168.0
181.10 163.0
181.10 158.0
181.10 153.0
181.10 148.0
181.10 143.0
181.10 138.0
181.10 133.0
181.10 128.0
181.10 123.0
181.10 118.0
181.10 113.0
181.10 108.0
181.10 103.0
181.10 98.0
181.10 93.0
181.10 88.0
181.10 83.0
181.10 78.0
181.10 73.0
181.10 68.0
181.10 63.0
181.10 58.0
181.10 53.0
181.10 48.0

Fig.6(s)

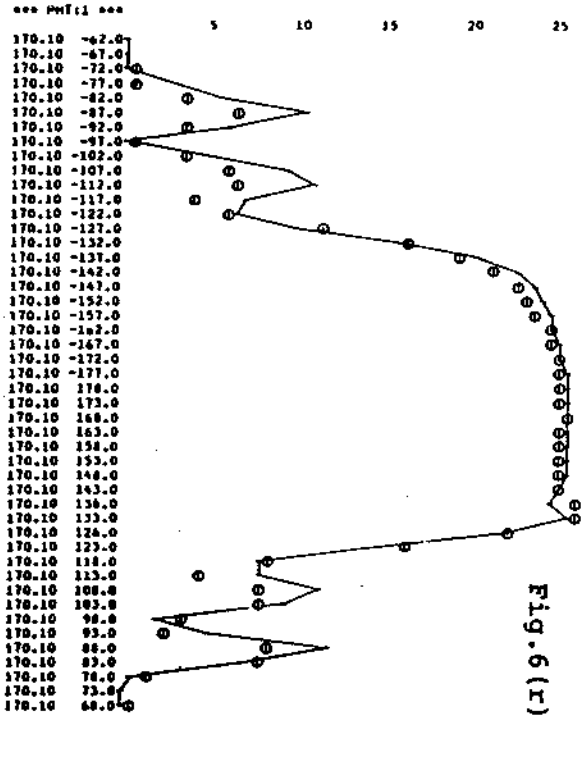
*** PHI:1 ***
5
10
15
20
25
170.10 -62.0
170.10 -67.0
170.10 -72.0
170.10 -77.0
170.10 -82.0
170.10 -87.0
170.10 -92.0
170.10 -97.0
170.10 -102.0
170.10 -107.0
170.10 -112.0
170.10 -117.0
170.10 -122.0
170.10 -127.0
170.10 -132.0
170.10 -137.0
170.10 -142.0
170.10 -147.0
170.10 -152.0
170.10 -157.0
170.10 -162.0
170.10 -167.0
170.10 -172.0
170.10 -177.0
170.10 176.0
170.10 173.0
170.10 168.0
170.10 163.0
170.10 158.0
170.10 153.0
170.10 148.0
170.10 143.0
170.10 138.0
170.10 133.0
170.10 128.0
170.10 123.0
170.10 118.0
170.10 113.0
170.10 108.0
170.10 103.0
170.10 98.0
170.10 93.0
170.10 88.0
170.10 83.0
170.10 78.0
170.10 73.0
170.10 68.0

Fig.6(r)

Fig.7

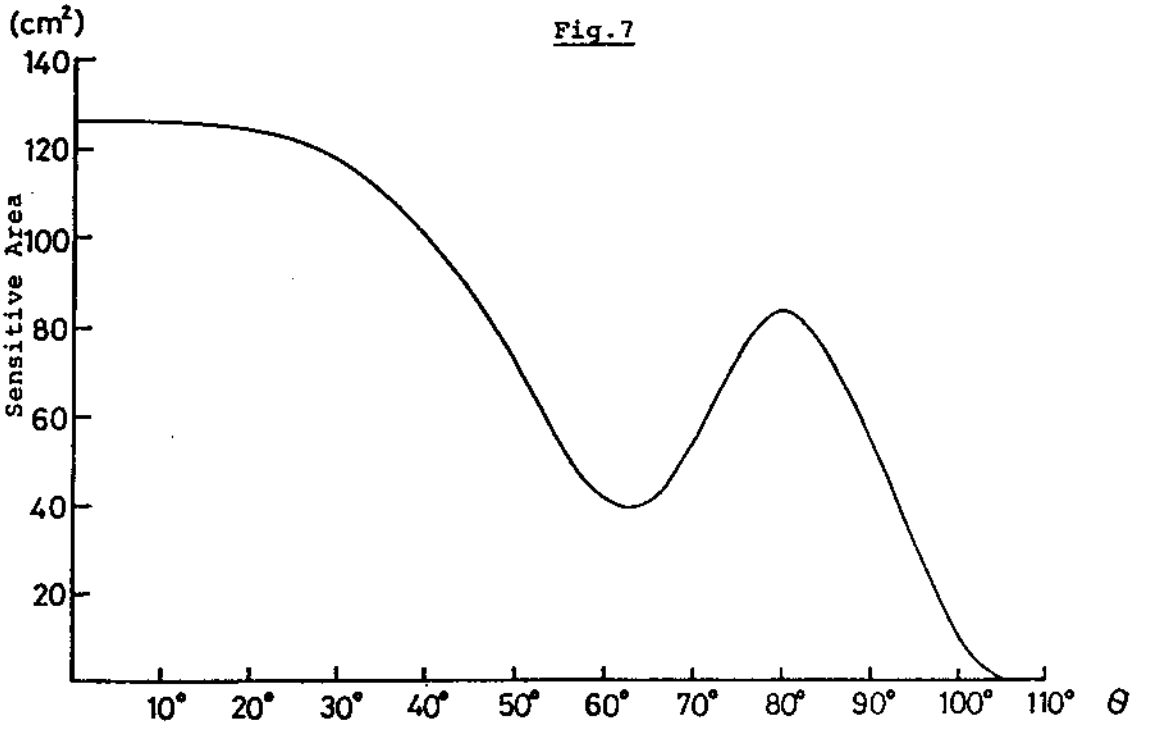
(cm²)
140
120
100
80
60
40
20
Sensitive Area
10°
20°
30°
40°
50°
60°
70°
80°
90°
100°
110°
θ

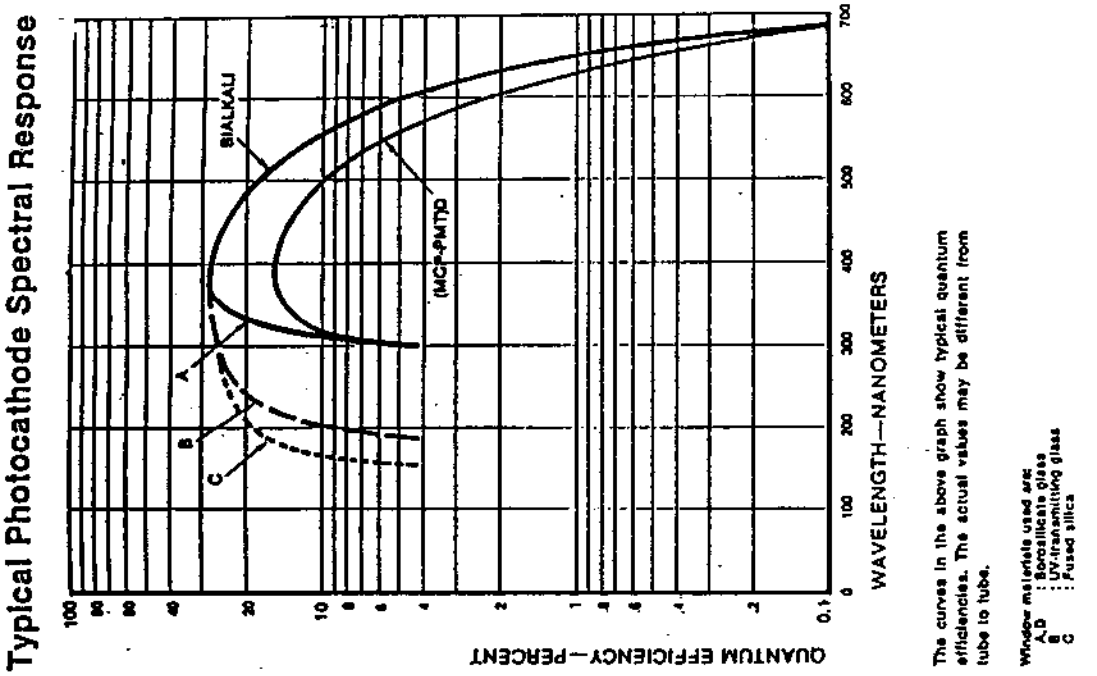
Typical Photocathode Spectral Response
BIALKALI
(MCP-PMT)D
A
B
C
QUANTUM EFFICIENCY—PERCENT
WAVELENGTH—NANOMETERS
The curves in the above graph show typical quantum efficiencies. The actual values may be different from tube to tube.
Window materials used are:
A,D : Borosilicate glass
B : UV-transmitting glass
C : Fused silica

Fig.8

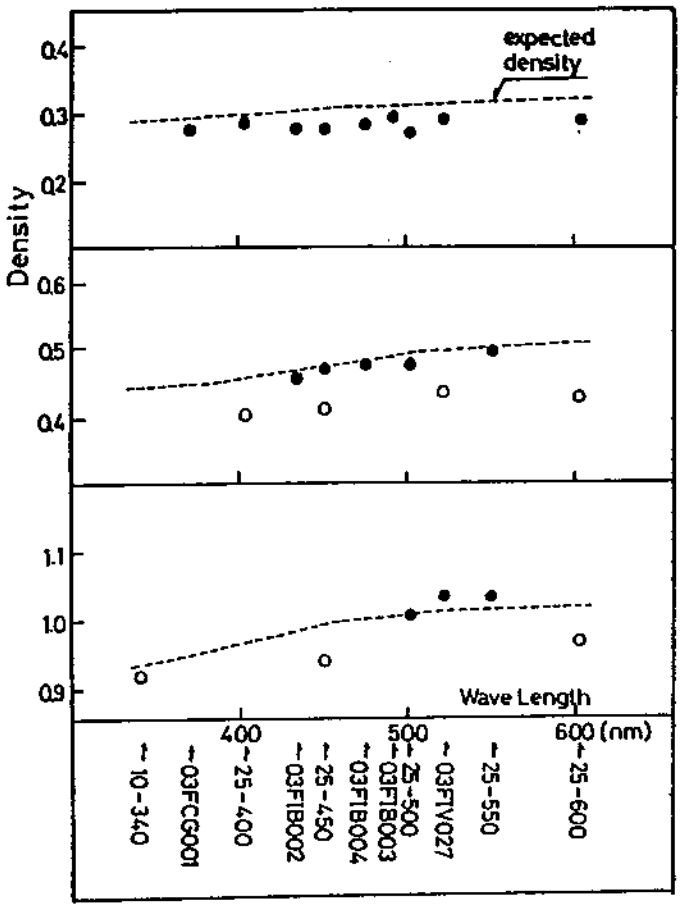
expected
density
Density
0.4
0.3
0.2
0.6
0.5
0.4
1.1
1.0
0.9
Wave Length
400
500
600 (nm)
~ 10-340
~03FCG001
~25-400
~03FIB002
~25-450
~03FIB004
~03FIB003
~25-500
~03FTV027
~25-550
~25-600

Fig.A1

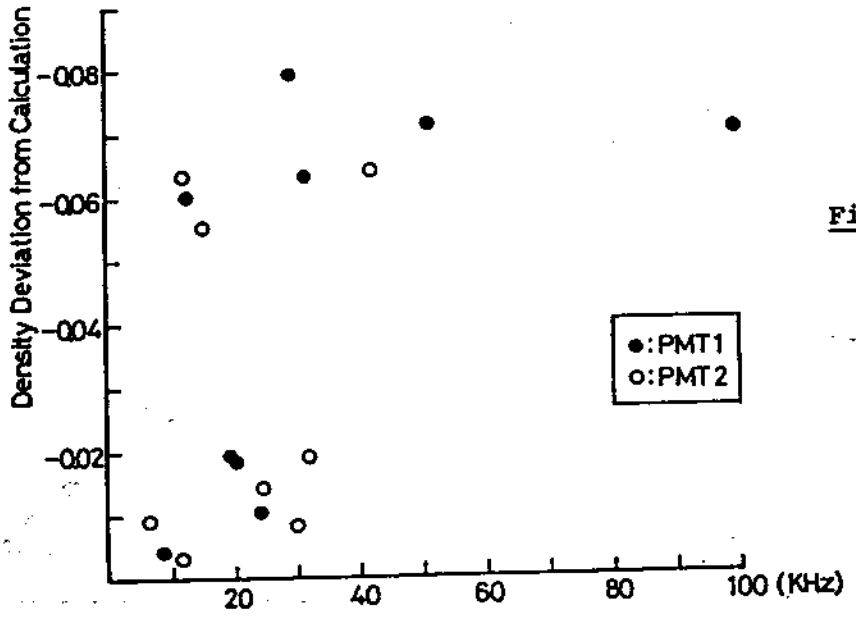
Density Deviation from Calculation
-0.08
-0.06
-0.04
-0.02
●:PMT1
○:PMT2
20
40
60
80
100 (KHz)

Fig.A2

Fig.A3

Fig.A3(a)

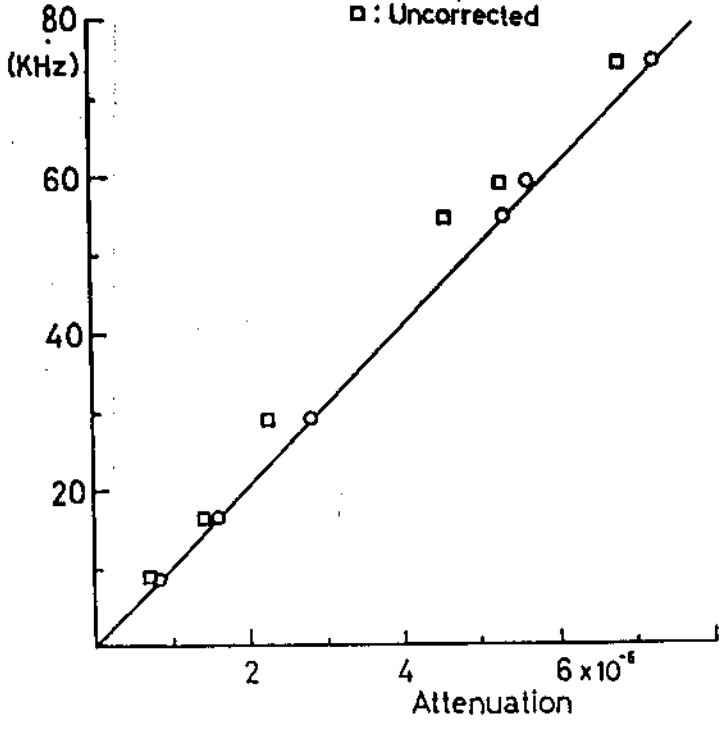

Fig.A3(b)

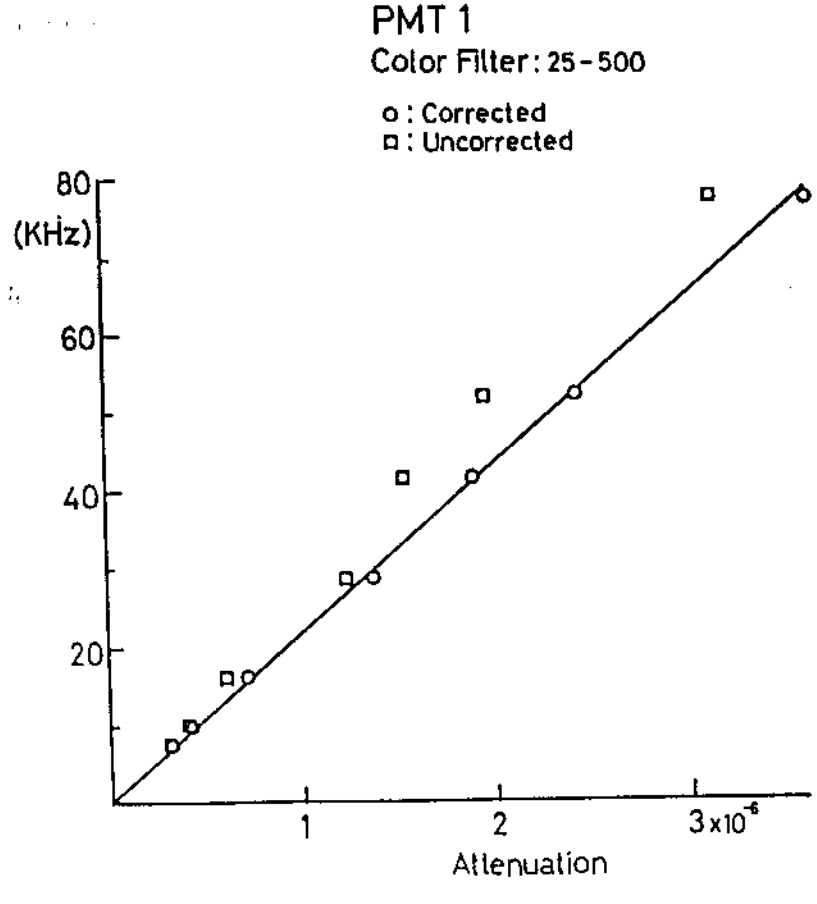

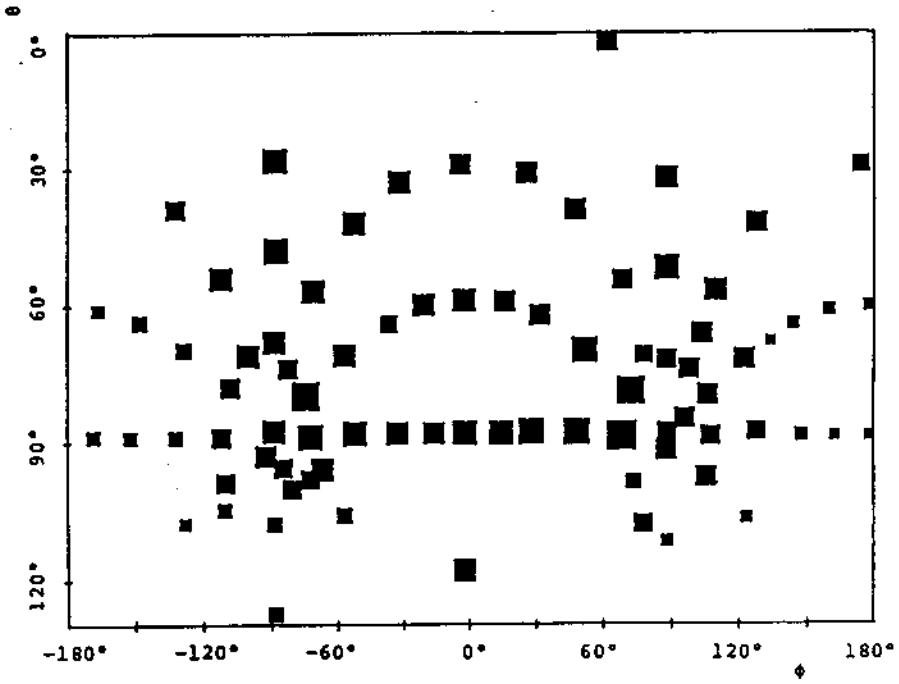
θ
0°
30°
60°
90°
120°
-180°
-120°
-60°
0°
60°
120°
180°
φ

Fig.B1

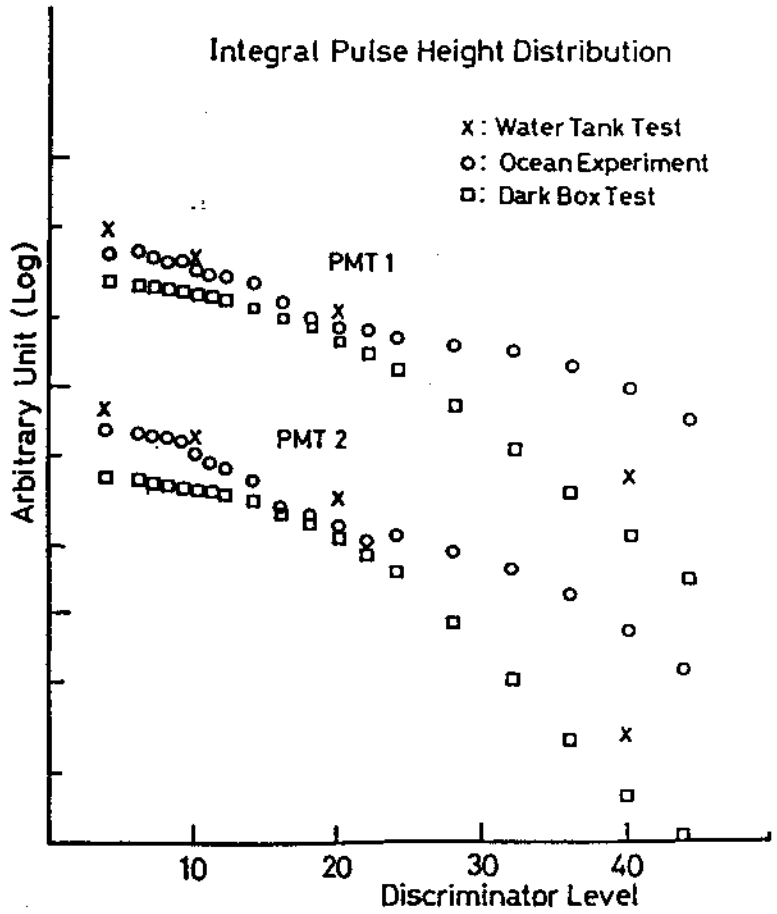
Integral Pulse Height Distribution
x : Water Tank Test
o : Ocean Experiment
□ : Dark Box Test
PMT 1
PMT 2
Arbitrary Unit (Log)
10
20
30
40
Discriminator Level

Fig.B2